

Short Communication

Electrodeposition of Superhydrophobic Hydroxyapatite/Magnesium Phosphate on a Magnesium Alloy Substrate for Enhanced Corrosion Resistance

Jiajun Huang

School of Civil Engineering and Architecture, Xinxiang University, Xinxiang, 453000, China

E-mail: huangjiajun_xx168@126.com

Received: 11 February 2017 / *Accepted:* 23 March 2017 / *Published:* 12 May 2017

Magnesium phosphate-doped hydroxyapatite and magnesium hydrogen phosphate-doped dicalcium phosphate dihydrate superhydrophobic coatings were electrolytically deposited on an AZ91D alloy. The contact angles of water/oil were 155°/141°, respectively. In comparison with the bare substrate, electrochemical measurements of the superamphiphobic surfaces, including both EIS measurement and potentiodynamic polarization curves, all demonstrated a dramatic enhancement in the inhibition of surface corrosion.

Keywords: Magnesium alloy; Electrodeposition; Hydroxyapatite; Superhydrophobic coating; Corrosion

1. INTRODUCTION

In recent years, magnesium alloys, characterized by outstanding physical and mechanical characteristics such as great specific stiffness and specific strength, metal removal performance, low density, excellent electromagnetic shielding, and high strength/weight ratio, have been applied in a variety of practical applications [1-3]. The AZ91D magnesium alloy has also been applied in many fields, such as aircrafts, cell phones and biomaterials [4, 5]. However, the development of its application has been adversely affected by its high metal reactivity and susceptibility to corrosion. With the purpose of achieving an extensive range of applications, researchers have devoted themselves to the improvement of the corrosion inhibition attributes of AZ91D magnesium alloys [6-8]. Every year, metal corrosion caused by metal interaction leads to huge economic losses [9]. Unfortunately, the prevention of corrosion itself is only minorly feasible, so the focus in this area is on decreasing the corrosion rate; many studies have concentrated on slowing the corrosion kinetics and/or modifying its

mechanism [10]. To date, approaches to control metal corrosion have generally employed cathodic protection, adopted corrosion inhibitors, developed coatings with protective effects, or combined these approaches. Inspired by self-cleaning lotus leaves and the water-resistant leg of one water strider, the adoption of superhydrophobic surfaces with water contact angles above 150° and sliding angles below 10° has been regarded as one of the promising approaches to enhance metal corrosion resistance. This is because these surfaces have the capacity to inhibit surface interactions with water or environmental moisture [11-13].

The adoption of Ca-P coatings to protect the surface of metals has been widely studied. The outstanding performance of Ca-P coatings has been demonstrated in several studies, as the anti-corrosion performance of magnesium alloys is improved in the presence of these coatings [14-21]. DCPD (dicalcium phosphate dihydrate, $\text{CaHPO}_4 \cdot 2\text{H}_2\text{O}$) and HA (hydroxyapatite, $\text{Ca}_{10}(\text{PO}_4)_6(\text{OH})_2$), favorable materials to protect biodegradable Mg alloys, are two of the most extensively investigated Ca-P coatings that can enhance the anti-corrosion property of Mg alloys [22-25]. At present, a variety of methods have been utilized to fabricate superhydrophobic surfaces on metal materials, such as electroplating [26, 27] on copper substrates as well as chemical corrosion [28, 29] on aluminum alloys, thus enhancing corrosion inhibition. In comparison with other metallic materials, the acquisition of superhydrophobic surfaces on magnesium alloys can be realized through various approaches, such as electrochemical deposition [30], chemical vapor deposition [31], chemical silver plating [32], chemical erosion [33], polymer plating [34-37], micro-arc oxidation [38] and anodization [39]. Electrodeposition, characterized by its diverse merits such as easy control, cost effectiveness, simplicity, and capability of forming a large surface area has become one of the most advantageous methods for the fabrication of superhydrophobic surfaces.

In this work, to enhance the anti-corrosion performance of HA, a magnesium phosphate (MP, $\text{Mg}_3(\text{PO}_4)_2$)-doped HA composite superhydrophobic coating was electrodeposited onto AZ91D. $\text{Mg}_3(\text{PO}_4)_2$ was adopted as the adulterant because of the resemblance between its chemical attributes and those of HA.

2. EXPERIMENTS

2.1. Materials

In this study, the samples were AZ91D magnesium alloy pieces cut to $25 \times 25 \times 10 \text{ mm}^3$, with a chemical composition as follows: Al 8.534 wt%, Zn 0.522 wt%, Mn 0.208 wt%, Si 0.016 wt%, Fe 0.002 wt%, Ni < 0.001 wt%, balance being Mg. Subsequently, these specimens were ground mechanically by using 500/1000/1500 grit emery papers and washed ultrasonically for 10 min each in pure ethanol and acetone.

2.2. Electrodeposition of DCPD, MHP, and DCPD-MHP

The electrodeposition of the DCPD, MgHPO_4 (MHP) and DCPD- MgHPO_4 (DCPD-MHP) coatings was accomplished on AZ91D magnesium alloy. The electrodeposition was conducted at room

temperature using a CHI 660B electrochemical workstation. In this process, a three-electrode cell was adopted, and the counter, reference and working electrodes were a platinum electrode, a saturated calomel electrode (SCE) and AZ91D magnesium alloy, respectively. The ampere density was altered to 0.5 mA/cm^2 and controlled over the entire electrodeposition course. Table 1 illustrates the electrolyte compositions. Each specimen was fully electrodeposited within 1000 s. When the deposition was complete, each coated AZ91D magnesium alloy was washed using distilled water and subsequently dried in an evacuated container.

Table 1. Composition of the electrolytes.

Components	DCPD (M)	MHP (M)	DCPD-MHP (M)
$\text{Ca}(\text{NO}_3)_2$	0.04	—	0.04
$\text{Mg}(\text{NO}_3)_2$	—	0.04	0.04
$(\text{NH}_4)_2\text{H}_2\text{PO}_4$	0.025	0.03	0.05
NaNO_3	0.1	0.1	0.1
H_2O_2	10	10	10

Subsequently, the DCPD-, MHP-, and DCPD-MHP-coated specimens were dipped into a 0.1 mol/L NaOH solution for 4 hours at $80 \text{ }^\circ\text{C}$ to transform them into HA, $\text{Mg}_3(\text{PO}_4)_2$ (MP) and $\text{HA-Mg}_3(\text{PO}_4)_2$ (HAMP), respectively. When the alkali treatment was finished, each specimen was washed with distilled water and subsequently dried in an evacuated container. For the comparison test, two groups of samples were subjected to experiments: the pre-transformation group, DCPD-, MHP-, and DCPD-MHP-coated specimens, and the after-transformation group, HA-, MP-, and HAMP-coated specimens.

2.3. Characterizations

The sample surface wetting properties were characterized by water/oil contact angles (CAs) using a contact angle meter (JC2000A Powereach, China) at room temperature. To examine the chemical composition of the surfaces, an X-ray diffractometer system (XRD, D/Max2500, Japan) was used.

2.4. Electrochemical analysis

The molding of each specimen was realized in epoxy resin, with a 4-cm^2 superficial area exposed to Hank's solution (NaCl 8.010 g/L, KCl 0.400 g/L, NaHCO_3 0.475 g/L, KH_2PO_4 0.060 g/L, glucose 1.000 g/L and $\text{Na}_2\text{HPO}_4 \cdot 12\text{H}_2\text{O}$ 0.126 g/L); the original pH value of this solution (the test medium) was 7.4. In these tests, the three-electrode cell adopted was in accordance with that applied in the electrodeposition process. Before the initiation of these tests, samples were washed using deionized

water, dried in air, and subsequently dipped in Hank's solution for 1 hour at 37 °C to stabilize their potential. After immersion for 1 hour, the initial scanning potential was set 300 mV lower than the stabilized potential. After this, the recording of the potentiodynamic polarization curves was performed at a scanning speed of 1 mV/s. Under the open circuit potential together with a sinusoidal wave whose amplitude was 10 mV, EIS tests were obtained over a frequency range of 10^5 to 10^{-2} at room temperature.

3. RESULTS AND DISCUSSION

XRD is applied widely and frequently in the analysis of the crystalline structure of materials. Figure 1A (DCPD-, MHP- and DCPD-MHP-coated samples) and Figure 1B (HA-, MP- and HAMP-coated samples) are the XRD patterns of the specimens studied. In the patterns, peaks in accordance with MgHPO_4 appeared, revealing that the electrodeposition of the MgHPO_4 coating onto the AZ91D magnesium alloy was successful. In addition, Figure 1A also exhibits peaks in accordance with Mg in the substrate. These peaks, caused by the transmission of X-rays, appear in the patterns of every coated specimen. Moreover, the appearance of DCPD peaks shows that on the AZ91D magnesium alloy surface, a DCPD coating with good crystallization was electrodeposited. Both DCPD and MgHPO_4 appear on the pattern of the DCPD-MHP-coated specimen, revealing a DCPD- MgHPO_4 composite coating on the alloy. The spectra of HA- and MP- exhibit $\text{Mg}_3(\text{PO}_4)_2$ as well as HA peaks, indicating the formation of HA and $\text{Mg}_3(\text{PO}_4)_2$ coatings on the AZ91D magnesium alloy after the DCPD and MHP coatings underwent the alkali-heat treatment. In the patterns of the HAMP specimen, HA and $\text{Mg}_3(\text{PO}_4)_2$ peaks appeared, manifesting the successful formation of an HA- $\text{Mg}_3(\text{PO}_4)_2$ composite coating on the as-prepared alloy.

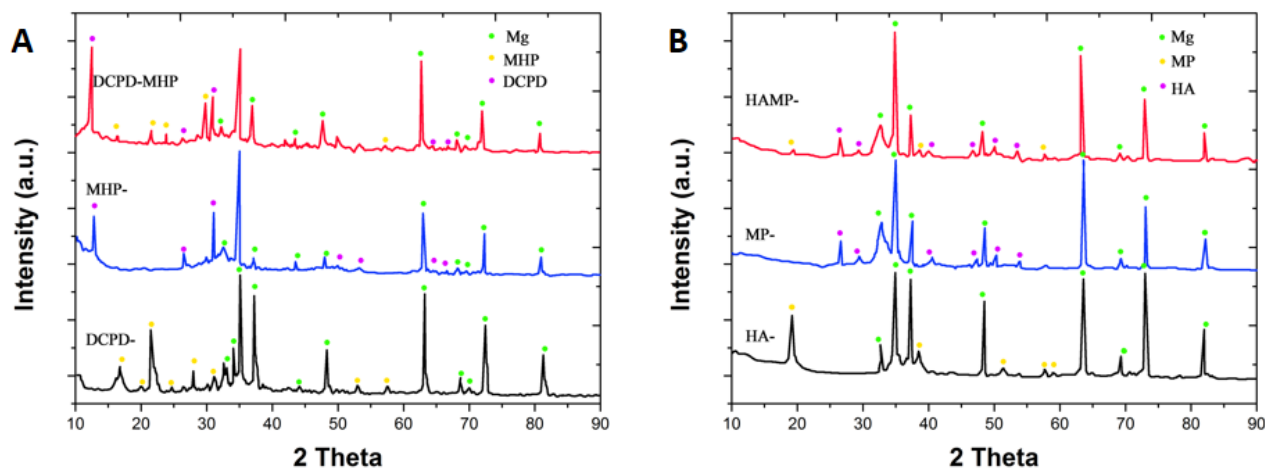


Figure 1. (A) XRD patterns of the DCPD-, MHP-, and DCPD-MHP-coated specimens as well as (B) the HA-, MP-, and HAMP-coated specimens.

Figure 2 illustrates the EDS analyses of the coating fabricated in this study. This figure shows that the main composition of the coating was Mg, Al, P and Ca and that the electrolytes were the source of Si and Ca in the coating.

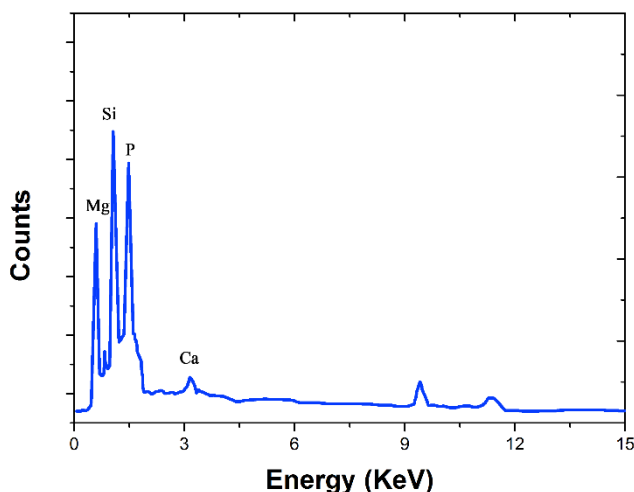


Figure 2. EDS analyses of the HAMP-coated specimen.

In the electrodeposition process of the Ca-P coating, H_2O_2 and H_2O molecules near the working electrode obtain electrons, leading to excess OH^- . The H_2O_2 in the electrolyte has a high potential to preferentially accept electrons instead of forming H_2 , thus eliminating the adverse impact of constantly generated gas on the electrodeposited coating. In addition, an enhancement of the coating uniformity may also be achieved. The resulting OH^- in the vicinity of the working electrode may react with H_2PO_4^- , thus producing HPO_4^{2-} . Then, HPO_4^{2-} may integrate with Ca^{2+} to be deposited as CaHPO_4 (DCPD) on the AZ91D magnesium alloy surface. Subsequently, through a parallel mechanism, the Mg-P coating would also be deposited. The acquired HPO_4^{2-} has a high potential to combine with Mg^{2+} , leading to the formation of MgHPO_4 which may then attach to the working electrode surface and develop an MHP coating. The deposition of the Ca-Mg-P composite coating was achieved in a similar way. That is, the HPO_4^{2-} would combine with the Mg^{2+} and Ca^{2+} at the same time in the electrolyte, giving rise to a $\text{CaHPO}_4\text{-MgHPO}_4$ complex coating. Under an acidic electrolyte (pH=4.4), Mg^{2+} is generated from the Mg substrate during the electrodeposition process, and later, for the purpose of developing MgHPO_4 , these ions would integrate with HPO_4^{2-} . To some extent, this shows that MgHPO_4 is produced in the preparation process of DCPD by means of electrodeposition, and therefore adding Mg^{2+} to the electrolyte should barely affect the development of MgHPO_4 . From the results gained, however, it can be seen that adding Mg^{2+} to the electrolyte can dramatically affect the development of MgHPO_4 . In the acidic electrolyte, the concentration of H^+ was $\sim 4 \times 10^{-5}$ mol/L (pH=4.4). In the electrodeposition process, OH^- would be formed constantly around the working electrode made of Mg such that there would a great deal of OH^- in the vicinity of the Mg substrate, and thus, it could be free from the damage of the corrosive electrolyte. Nearly all of the H_2 generated around the substrate caused by the interaction between the electrons and H^+ came from the electrochemical workstation instead of the substrate's electrons. In electrodeposition, only a small

amount of Mg^{2+} would be formed from the substrate, in which the development of MgHPO_4 was barely possible without the addition of Mg^{2+} . As a result, in the preceding studies, there were no MgHPO_4 peaks observed in the XRD pattern of the electrodeposited DCPD.

In the study, we investigated the wettability performance of diverse coatings (water/oil). It can be seen in Figure 3 that the fabricated coating with micro/nanoscale cauliflower-like cluster binary structures possessed very great contact angles (CAs) to water as well as oil, 155° and 141° , respectively, when a HAMP coating developed on the surface. Apparently, in the formation of the HA-coating, the CAs (water/oil) were improved dramatically. After the development of the HAMP coating, the surface revealed superamphiphobic (both superhydrophobic and superoleophobic) attributes. The united microstructure of the surface of the coating would be expected to have the capacity to obtain air with high efficiency, thereby avoiding interaction between water drops and the surface and thus decreasing the rate at which the corrosive medium originating from the water droplets would corrode the substrate. Compared to a previously published similar investigation [40], the results demonstrated in this work show the proposed coating to exhibit an excellent superoleophobic performance.

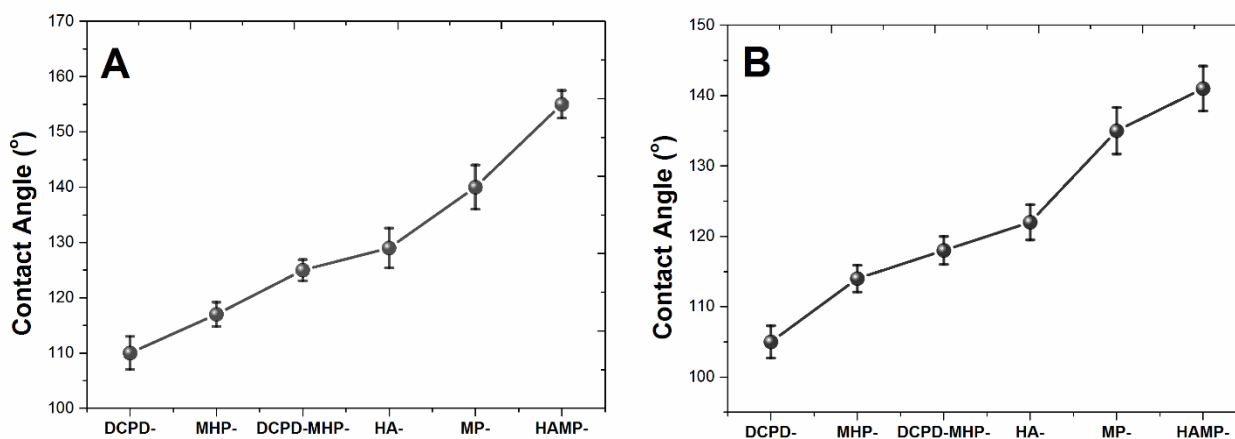


Figure 3. Changes in the (A) water and (B) oil contact angles of the specimens' surfaces at different coating phases.

With the purpose of studying the corrosion inhibition attributes of the samples, we used potentiodynamic polarization curves to perform the characterization in a 3.5 wt% NaCl solution. The corrosion potential (E_{corr}) and corrosion current density (i_{corr}) were derived directly from the polarization curves by Tafel region extrapolation. In general, the cathodic polarization curve is attributed to the hydrogen evolution reaction due to the reduction of water, while the anodic polarization curve is associated with the dissolution of Mg, leading to the formation of Mg^{2+} [41]. As seen in Figure 5, to determine the values of E_{corr} (vs. Ag/AgCl) and i_{corr} , we utilize the calculated anodic Tafel lines as well as the extrapolation of linear Tafel segments. Concerning the vacant substrate as well as the amphiphobic coating on the magnesium alloy, it can be seen in Table 2 that in comparison with the vacant substrate, the superamphiphobic coating's corrosion potential E_{corr}

revealed a positive displacement, namely from -1.46 V to -0.795 V. This results from the protective attributes of the hydrophobic coating developed on the substrate. Table 2 shows the polarization parameters of the bare AZ91D magnesium alloy as well as the HAMP-coated specimen and the corresponding inhibition efficiencies. At the same time, there was a decline in the corrosion current density of the superamphiphobic coating of approximately 1 order of magnitude in comparison with that of the vacant specimen. Nevertheless, passivation current can also be found in the surface of the superamphiphobic specimen, demonstrating that the film on the substrate had promoted the inhibition of the surface corrosion. Consequently, an enhancement of the anti-corrosion performance of the substrate can be realized through superamphiphobic coating.

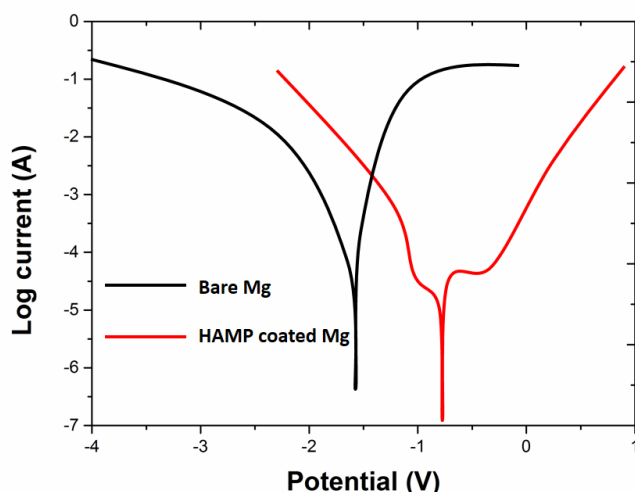


Figure 4. Polarization curves of the bare AZ91D magnesium alloy and the HAMP-coated specimen.

Table 2. Electrochemical polarization parameters for the bare AZ91D magnesium alloy and HAMP-coated specimen.

Sample	E_{corr} (mV)	I_{corr} (mA/cm ²)	b_a (mV/dec)	b_c (mV/dec)	Inhibition efficiency
Bare AZ91D magnesium alloy	-1211	3.41	95	108	-
HAMP-coated AZ91D	-650	1.60	97	104	87.5

Table 3. Electrochemical impedance parameters deduced from Nyquist plots.

Samples	R_{ct} (k Ω /cm ²)	CPE_{d1} (μ F/cm ²)	CPE_{d2} (μ F/cm ²)	R_s (Ω /cm ²)	R_c (k Ω /cm ²)
Bare AZ91D Mg alloy	3.9	4.51	—	14.06	—
HAMP-coated AZ91D Mg alloy	45.7	19.22	45.22	233.5	8.6

Figure 5 shows the Nyquist plots of the bare magnesium alloy and the superamphiphobic samples in a 3.5 wt% NaCl water solution. For the clean AZ91D magnesium alloy substrate, the Nyquist plot comprised double capacitive loops, which accord with the medium-high and the low frequency areas, respectively. Because the Mg alloy substrate contains several different metal elements, such as Mg, Al and Mn, the outer surface of the alloy should have a layered structure composed of metal oxides, and the Nyquist plot of the naked electrode should show two semicircles [42]. As seen in Figure 6A, the phase Bode plots conformed with this expectation. However, the Nyquist plots of the superamphiphobic coating contained only one capacitive loop, whose diameter had a proportional relation with the corrosion rate. This result clearly showed that in the 3.5 wt% NaCl solution, the superamphiphobic samples possessed relatively higher corrosion inhibition than the clean AZ91D magnesium alloy substrate. In addition, assisted by the impedance modulus values revealed in the Bode plots, the measurement of the corrosion rate can be realized. In this work, Bode plots were adopted to complete the exploration. As seen in Figure 6, the superhydrophobic surface possessed a larger impedance modulus at low frequency compared to the bare substrate, with a value nearly one order of magnitude greater than that of the bare substrate, just as mentioned earlier. This signified that the anti-corrosion performance of the substrate can be strengthened remarkably by the superamphiphobic coating. Moreover, the phase diagram can be further observed in Figure 6B, exhibiting a broad wave crest approaching 90° at the intermediate frequency. Based on the measurement results, the conclusion can be drawn that the superamphiphobic surface has a positive effect on the improvement of the corrosion inhibition, helping maintain the damping capacity. It is highly likely that the air layer formed on the surface of the superamphiphobic layer facilitates the corrosion inhibition, as it can greatly block the permeation of the corrosive solution. The results obtained proved that the superamphiphobic surfaces can help the magnesium alloy substrate avoid corrosion, corresponding to the results of the potentiodynamic polarization test.

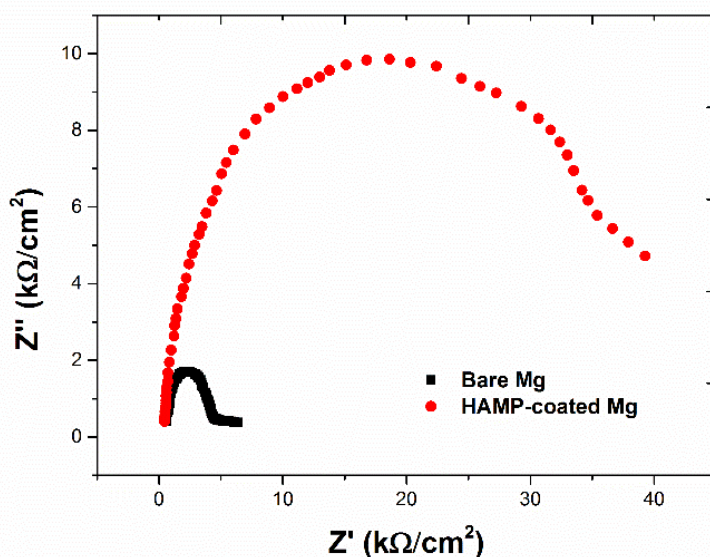


Figure 5. Nyquist plots of bare AZ91D magnesium alloy and the HAMP-coated specimen in 3.5 wt% NaCl water solution.

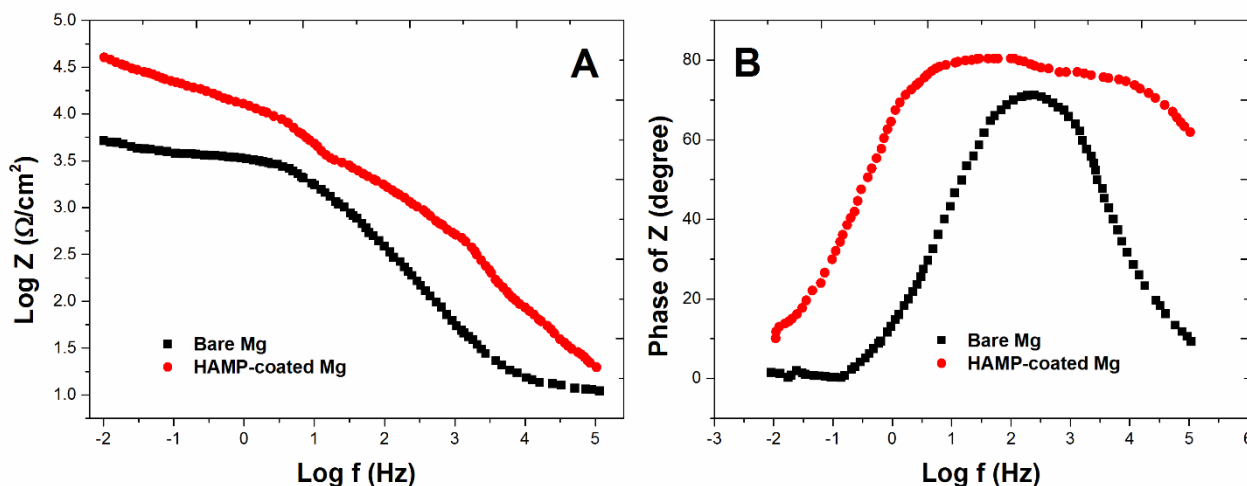


Figure 6. Bode plots of bare AZ91D magnesium alloy and the HAMP-coated sample in 3.5 wt% NaCl water solution.

4. CONCLUSIONS

Electrochemical and immersion tests strongly demonstrated the enhancement of anti-corrosion performance from a HAMP superhydrophobic coating on AZ91D magnesium alloy prepared through electrodeposition with a subsequent alkali-heat treatment. The water and oil contact angles of the acquired surfaces were 155° and 141° , respectively. In comparison with the bare substrate, the superamphiphobic surface electrochemical measurements, including both EIS measurement and potentiodynamic polarization curves, all reflected the dramatic improvement of the surface corrosion inhibition, which can greatly protect the magnesium alloy substrate from corrosion.

References

1. H. Wang, L. Chen, B. Liu, X. Li, J. Wang and Q. Jiang, *Materials Chemistry & Physics*, 135 (2012) 358.
2. S. Thakur, B. Dhindaw, N. Hort and K. Kainer, *Metallurgical and Materials Transactions A*, 35 (2004) 1167.
3. Z. Yong, Z. Jin, Q. Cheng and Y. Liu, *Appl. Surf. Sci.*, 255 (2008) 1672.
4. N. Li and Y. Zheng, *Journal of Materials Science & Technology*, 29 (2013) 489.
5. M. Liu, P.J. Uggowitzer, P. Schmutz and A. Atrens, *JOM*, 60 (2008) 39.
6. T. Zhang, Y. Shao, G. Meng, Z. Cui and F. Wang, *Corrosion Science*, 53 (2011) 1960.
7. H. Huo, Y. Li and F. Wang, *Corrosion Science*, 46 (2004) 1467.
8. L. Wang, J. Shen, Z. Feng and H. Fu, *Applied Physics A*, 113 (2013) 177.
9. R. Zuo, *Applied Microbiology and Biotechnology*, 76 (2007) 1245.
10. C. Peng, K. Chang, C. Weng, M. Lai, C. Hsu, S. Hsu, Y. Hsu, W. Hung, Y. Wei and J. Yeh, *Electrochimica Acta*, 95 (2013) 192.
11. T. Ishizaki, Y. Masuda and M. Sakamoto, *Langmuir the Acs Journal of Surfaces & Colloids*, 27 (2011) 4780.

12. Q. Liu and Z. Kang, *Mater. Lett.*, 137 (2014) 210.
13. C. Gu and J. Tu, *Langmuir*, 27 (2011) 10132.
14. E. Abdel-Aal, D. Dietrich, S. Steinhäuser and B. Wielage, *Surface & Coatings Technology*, 202 (2008) 5895.
15. S. Hiromoto, E. Onodera, A. Chiba, K. Asami and T. Hanawa, *Biomaterials*, 26 (2005) 4912.
16. X. Chen, M. Zhang, X. Pu, G. Yin, X. Liao, Z. Huang and Y. Yao, *Surface & Coatings Technology*, 249 (2014) 97.
17. C. Zhang, R. Zeng, C. Liu and J. Gao, *Surface & Coatings Technology*, 204 (2010) 3636.
18. B. Lin, M. Zhong, C. Zheng, L. Cao, D. Wang, L. Wang, J. Liang and B. Cao, *Surface & Coatings Technology*, 281 (2015) 82.
19. H. Wang, S. Zhu, L. Wang, Y. Feng, X. Ma and S. Guan, *Appl. Surf. Sci.*, 307 (2014) 92.
20. H. Tang, D. Yu, Y. Luo and F. Wang, *Appl. Surf. Sci.*, 264 (2013) 816.
21. Z. Yao, L. Li and Z. Jiang, *Appl. Surf. Sci.*, 255 (2009) 6724.
22. D. Sreekanth and N. Rameshbabu, *Mater. Lett.*, 68 (2011) 439.
23. Y. Kuboki, H. Takita, D. Kobayashi, E. Tsuruga, M. Inoue, M. Murata, N. Nagai, Y. Dohi and H. Ohgushi, *Journal of Biomedical Materials Research*, 39 (1998) 190.
24. H. Simank, M. Stuber, R. Frahm, L. Helbig, H. Lenthe and R. Müller, *Biomaterials*, 27 (2006) 3988.
25. J. Thanner, J. Kärrholm, P. Herberts and H. Malchau, *Journal of Arthroplasty*, 15 (2000) 405.
26. H. Tao, A. Hu, H. Ling, L. Ming and D. Mao, *Appl. Surf. Sci.*, 256 (2010) 2400.
27. C. Zhi, L. Hao, A. Chen, Q. Song and C. Chen, *Electrochimica Acta*, 59 (2012) 168.
28. X. Yan, J. Chen, J. Yang, Q. Xue and P. Miele, *ACS Applied Materials & Interfaces*, 2 (2010) 2521.
29. L. Liu, J. Zhao, Z. Yi, Z. Fan and Y. Zhang, *Journal of Colloid & Interface Science*, 358 (2011) 277.
30. Y. Liu, X. Yin, J. Zhang, S. Yu, Z. Han and L. Ren, *Electrochimica Acta*, 125 (2014) 395.
31. J. Zhang, Y. Wang, X. Wang, G. Ding, Y. Pan, H. Xie, Q. Chen and R. Cheng, *Journal of Applied Polymer Science*, 131 (2014) 378.
32. J. Jia, J. Fan, B. Xu and H. Dong, *Journal of Alloys & Compounds*, 554 (2013) 142.
33. J. Ou, W. Hu, M. Xue, F. Wang and W. Li, *ACS Applied Materials & Interfaces*, 5 (2013) 3101.
34. Z. Kang, X. Lai, J. Sang and Y. Li, *Thin Solid Films*, 520 (2011) 800.
35. Y. Sun, C. Kang, F. Liu and L. Song, *Drug Development Research*, 77 (2016) 393.
36. Y. Sun, C. Kang, Z. Yao, F. Liu and Y. Zhou, *Nano LIFE*, 6 (2016) 1642004.
37. Y. Sun, C. Kang, A. Zhang, F. Liu, J. Hu, X. Zhong and J. Xie, *European Journal of BioMedical Research*, 2 (2016) 12.
38. S. Wang, X. Guo, Y. Xie, L. Liu, H. Yang, R. Zhu, J. Gong, L. Peng and W. Ding, *Surface & Coatings Technology*, 213 (2012) 192.
39. G. Wang, Z. Guo and W. Liu, *Journal of Bionic Engineering*, 11 (2014) 325.
40. B. Li, Y. Chen, W. Huang, W. Yang, X. Yin and Y. Liu, *Ceram. Int.*, 42 (2016) 13074.
41. J. Chang, X. Guo, P. Fu, L. Peng and W. Ding, *Electrochimica Acta*, 52 (2007) 3160.
42. Z. Yong, J. Zhu, C. Qiu and Y. Liu, *Appl. Surf. Sci.*, 255 (2008) 1672.